Percolation as a Basic Concept for Macroscopic Capillarity

R. Hilfer and F. Doster

Institute for Computational Physics
Universität Stuttgart, 70569 Stuttgart, Germany

originally published in: Transport in Porous Media, Vol. 82, Issue 3, pages 507-519 (2010)
originally submitted: July 23rd, 2009

Abstract

The concepts of relative permeability and capillary pressure are crucial for the accepted traditional theory of two phase flow in porous media. Recently a theoretical approach was introduced that does not require these concepts as input [25, 26]. Instead it was based on the concept of hydraulic percolation of fluid phases. This paper presents the first numerical solutions of the coupled nonlinear partial differential equations introduced in [26]. Approximate numerical results for saturation profiles in one spatial dimension have been calculated. Long time limits of dynamic timedependent profiles are compared to stationary solutions of the traditional theory. The initial and boundary conditions are chosen to model the displacement processes that occur when a closed porous column containing two immiscible fluids of different density is raised from a horizontal to a vertical position in a gravitational field. The nature of the displacement process may change locally in space and time between drainage and imbibition. The theory gives local saturations for nonpercolating trapped fluids near the endpoint of the displacement.

Contents

[page 507, § 1]

1. Introduction

[507.1.1] Almost all accepted and applied theories of multiphase flow in porous media are based on generalized Darcy laws and the concurrent concept of relative permeabilities [43]. *[507.1.2]* Despite the fact that Wyckoff and Botset (1936) strongly emphasized the viriation of hydraulically disconnected fluid regions [30], almost all subsequent applications of the relative permeability concept treat the residual nonwetting (or irreducible wetting) saturations as material constants [5, 11, 16, 20, 32, 39, 42].

[page 508, § 1] *[508.2.1]* Modern theories of multiphase flow in porous media often resort to microscopic models (e.g., network models) [6, 8, 9, 13, 14, 17, 18, 21, 22, 31, 38]. *[508.2.2]* An important motivation is the need to derive or estimate macroscopic relative permeabilities from pore scale parameters. *[508.2.3]* It was emphasized in [43], however, that the "possibility of determining the overall dynamical behavior of nonhomogeneous fluids from a study of microscopic detail" is remote [43, p. 326]. *[508.2.4]* One should instead consider saturation, velocities, and pressure gradient "to derive therefrom the overall or macroscopic behavior of the system" [43]. *[508.2.5]* Rather surprisingly, the authors of [43] emphasize the important difference between "continouos moving" fluids and "stationary or locked" fluids in their introduction, but later cease to distinguish between them in the main body of the paper. *[508.2.6]* Experimentally, the volume fraction of stationary, locked, trapped, or nonpercolating fluid phases varies strongly with time and position [1, 3, 41, 43]. *[508.2.7]* Modeling such variations of trapped or nonpercolating fluid phases explicitly is the main objctive of this paper.

[508.3.1] Dispersed droplets, bubbles, or ganglia of one fluid phase obstruct the motion of the other fluid phase. *[508.3.2]* Extensive experimental and theoretical studies of the simple phenomenon exist [4, 19, 30, 33–37]. *[508.3.3]* It is, therefore, surprising that the concept of hydraulic percolation has been neglected in the modeling of two phase flow until 10 years ago [23].

[508.4.1] Given that the basic concept of hydraulic percolation for macroscpic capillarity has been discussed extensively in [24–26] our objective in this paper is to find approximate numerical solutions of the mathematical model. *[508.4.2]* Let us, therefore begin the discussion by formulating a set of mathematical equations for the hydraulic percolation approach in Sect. 2. *[508.4.3]* One also needs to specify initial and boundary conditions representing a realistic experiment. *[508.4.4]* Raising a closed column from a horizontal to a vertical orientation causes simultaneous imbibition and drainage processes inside the medium as emphasized already in [26]. *[508.4.5]* In this paper, we report approximate numerical results for the full time evolution of such simultaneous imbibition and drainage processes. *[508.4.6]* As expected, the resulting equilibrium saturations depend strongly on the initial conditions. *[508.4.7]* Moreover, they differ significantly from the equilibrium profiles of the traditional theory.

2. Formulation of the Model

2.1. Balance Laws

[508.5.1] Consider a onedimensional, homogeneous, isotropic and incompressible porous column filled with two immiscible Newtonian fluids. *[508.5.2]* In a one dimensional model transversal variations and column thickness are neglected. *[508.5.3]* Let $S_{\mathbb{W}} = S_{\mathbb{W}}(x,t)$ denote the saturation of wetting fluid (called water), and $S_{\mathbb{O}} = S_{\mathbb{O}}(x,t)$ the saturation of nonwetting fluid (called oil). *[508.5.4]* Here time is $t \geq 0$, and $x \in [0, L]$ is the position in a column of length L. *[508.5.5]* Each of the two fluid phases is considered to consist of a continuous, mobile, percolating subphase, and of a discontinuous, isolated, trapped or nonpercolating subphase as discussed in [23–26, 28]. *[508.5.6]* Following the notation of [26] the percolating phase of water is *[page 509, §0]* indexed by $i = 1$ and its nonpercolating phase is indexed by $i = 2$. *[509.0.1]* The water saturation is then $S_{\mathbb{W}} = S_1 + S_2$. *[509.0.2]* The percolating oil phase is indexed as $i = 3$ and its nonpercolating phase by $i = 4$. *[509.0.3]* The oil saturation is $S_{\mathbb{O}} = S_3 + S_4$. *[509.0.4]* The volume fraction ϕ_i of phase i is defined as $\phi_i = \phi S_i$ where the volume fraction of the pore space, also called porosity, is ϕ. *[509.0.5]* The volume fraction of the solid matrix is denoted as $\phi_5 = 1 - \phi$. *[509.0.6]* Volume conservation requires

$$\phi_1 + \phi_2 + \phi_3 + \phi_4 + \phi_5 = 1 \tag{1a}$$

$$S_1 + S_2 + S_3 + S_4 = 1 \tag{1b}$$

to hold.

[509.1.1] The mass balance of fluid phase i can be expressed in differential form as

$$\frac{\partial(\phi_i \varrho_i)}{\partial t} + \frac{\partial(\phi_i \varrho_i v_i)}{\partial x} = M_i \tag{2}$$

where $\varrho_i(x,t), \phi_i(x,t), v_i(x,t)$ are mass density, volume fraction and velocity of phase i as functions of position $x \in \mathbb{S} = [0, L] \subset \mathbb{R}$ and time $t \in \mathbb{R}_+$. *[509.1.2]* M_i is the mass transfer rate from all other phases into phase i.

[509.2.1] The momentum balance is written as ($i = 1, 2, 3, 4$)

$$\phi_i \varrho_i \frac{\mathrm{D}^i}{\mathrm{D}t} v_i - \phi_i \frac{\partial \Sigma_i}{\partial x} - \phi_i F_i = m_i - v_i M_i \tag{3}$$

where Σ_i is the stress tensor in the ith phase, F_i is the body force per unit volume acting on the ith phase, m_i is the momentum transfer into phase i from all the other phases, and $\mathrm{D}^i/\mathrm{D}t = \partial/\partial t + v_i \partial/\partial x$ denotes the material derivative for phase i. *[509.2.2]* The stress tensor for the nonpercolating phases is defined as the momentum flux across surfaces in the threedimensional continuum (see [29] for more discussion).

2.2. Constitutive Assumptions

[509.3.1] For a macroscopically homogeneous porous medium

$$\phi(x) = \phi = \text{const} \tag{4}$$

is assumed. *[509.3.2]* Incompressible fluids are assumed so that their densities

$$\varrho_1(x,t) = \varrho_{\mathbb{W}} \tag{5a}$$

$$\varrho_2(x,t) = \varrho_{\mathbb{W}} \tag{5b}$$

$$\varrho_3(x,t) = \varrho_{\mathbb{O}} \tag{5c}$$

$$\varrho_4(x,t) = \varrho_{\mathbb{O}} \tag{5d}$$

are independent of x, t.

[509.4.1] The percolating and the nonpercolating phases are able to exchange mass through breakup and coalescence of droplets, ganglia and clusters. *[509.4.2]* The mass transfer rates must depend on rates of saturation change. *[509.4.3]* They are here assumed to be

$$M_1 = -M_2 = \eta_2 \phi \varrho_{\mathbb{W}} \left(\frac{S_2 - {S_2}^*}{{S_{\mathbb{W}}}^* - S_{\mathbb{W}}} \right) \frac{\partial S_{\mathbb{W}}}{\partial t} \tag{6a}$$

$$M_3 = -M_4 = \eta_4 \phi \varrho_{\mathbb{O}} \left(\frac{S_4 - {S_4}^*}{{S_{\mathbb{O}}}^* - S_{\mathbb{O}}} \right) \frac{\partial S_{\mathbb{O}}}{\partial t} \tag{6b}$$

[page 510, §0] where η_2, η_4 are constants. *[510.0.1]* The parameters ${S_{\mathbb{W}}}^*, {S_{\mathbb{O}}}^*, {S_2}^*, {S_4}^*$ are defined by

$${S_{\mathbb{W}}}^* = (1 - S_{\mathbb{O}\,\mathrm{r}})\Theta\left(\partial_t S_{\mathbb{W}}\right) + S_{\mathbb{W}\,\mathrm{i}}\left[1 - \Theta\left(\partial_t S_{\mathbb{W}}\right)\right] \tag{7a}$$

$${S_{\mathbb{O}}}^* = 1 - {S_{\mathbb{W}}}^* \tag{7b}$$

$${S_2}^* = S_{\mathbb{W}\,\mathrm{i}}\left[1 - \Theta\left(\partial_t S_{\mathbb{W}}\right)\right] \tag{7c}$$

$${S_4}^* = S_{\mathbb{O}\,\mathrm{r}}\Theta\left(\partial_t S_{\mathbb{W}}\right) \tag{7d}$$

where $S_{\mathbb{W}\,\mathrm{i}}, S_{\mathbb{O}\,\mathrm{r}}$ are limiting saturations for S_2, S_4. *[510.0.2]* In eq. (7) the shorthand $\partial_t = \partial/\partial t$ is used and

$$\Theta(x) = \begin{cases} 1 & \text{for } x > 0, \\ 0 & \text{for } x \leq 0, \end{cases} \tag{8}$$

denotes the Heaviside unit step function. *[510.0.3]* Equation (7) follows from the form used in [26] for small rates of saturation change. *[510.0.4]* The mass exchange depends on the sign of $\partial_t S_{\mathbb{W}}$. *[510.0.5]* The sign determines the type of process. *[510.0.6]* It can switch locally between drainage and imbibition. *[510.0.7]* This results in hysteresis. *[510.0.8]* The structure of the mass exchange term was chosen with hindsight such that theoretical results obtained in the residual decoupling approximation agree with experimental measurements of capillary pressure. *[510.0.9]* The mass exchange terms have recently been further generalized to reproduce not only capillary pressure, but also experimental capillary desaturation curves [27].

[510.1.1] Turning to the momentum balance, note first that the inertial term will not be neglected in this paper. *[510.1.2]* The stress tensor for the four phases are specified as

$$\Sigma_1 = -P_1 \tag{9a}$$

$$\Sigma_2 = -P_3 + \gamma P_2^* S_2^{\gamma - 1} \tag{9b}$$

$$\Sigma_3 = -P_3 \tag{9c}$$

$$\Sigma_4 = -P_1 + \delta P_4^* S_4^{\delta - 1} \tag{9d}$$

where P_1 and P_3 are the fluid pressures in the percolating phases. *[510.1.3]* The constants P_2^*, P_4^* and exponents γ, δ are constitutive parameters. *[510.1.4]* The assumptions for the nonpercolating phases reflect their modified pressure. *[510.1.5]* This phenomenon seems to have been observed in experiment [2, Fig. 2, p. 233]. [a] *[510.1.6]* In applications, the parameters P_2^*, P_4^* and γ, δ are determined by measuring capillary pressure curves (see below). *[510.1.7]* The body forces are assumed to be given by gravity and capillarity. *[510.1.8]* They are specified as

$$F_1 = \varrho_1 g \sin\vartheta \tag{10a}$$

$$F_2 = \varrho_2 g \sin\vartheta + \Pi_\mathrm{a} \frac{\partial S_1^{-\alpha}}{\partial x} \tag{10b}$$

$$F_3 = \varrho_3 g \sin\vartheta \tag{10c}$$

$$F_4 = \varrho_4 g \sin\vartheta + \Pi_\mathrm{b} \frac{\partial S_3^{-\beta}}{\partial x} \tag{10d}$$

with constitutive constants $\Pi_\mathrm{a}, \Pi_\mathrm{b}$ and exponents $\alpha, \beta > 0$. *[510.1.9]* The angle $0 \leq \vartheta \leq \pi/2$ is the angle between the direction of the column and the direction of gravity with $\vartheta = \pi/2$ *[page 511, §0]* corresponding to alignment. *[511.0.1]* In applications the parameters $\Pi_\mathrm{a}, \Pi_\mathrm{b}$ and α, β are determined by measuring capillary pressure curves. *[511.0.2]* The capillary body forces in eqs. (10) reflect the wetting properties of the medium. *[511.0.3]* They oppose gravity and reduce buoyancy driven flows of the disconnected phases. *[511.0.4]* This is illustrated in the figures below.

[511.1.1] Finally, the momentum transfer terms are assumed to be given by linear viscous drag characterized by constitutive resistance coefficients R_{ij} through the equations

$$m_1 = R_{13}(v_3 - v_1) + R_{14}(v_4 - v_1) - R_{15} v_1 \tag{11a}$$

$$m_2 = R_{23}(v_3 - v_2) + R_{24}(v_4 - v_2) - R_{25} v_2 \tag{11b}$$

$$m_3 = R_{31}(v_1 - v_3) + R_{32}(v_2 - v_3) - R_{35} v_3 \tag{11c}$$

$$m_4 = R_{41}(v_1 - v_4) + R_{42}(v_2 - v_4) - R_{45} v_4 \tag{11d}$$

where $R_{12} = 0$ and $R_{34} = 0$ was used because there is no common interface and hence no direct viscous interaction between these phase pairs. *[511.1.2]* Remember that the index $i = 5$ represents the rock matrix. *[511.1.3]* For more details on these constitutive assumptions the reader is referred to the original papers [24–26].

[511.2.1] The balance laws (1b), (2) and (3) combined with the constitutive assumptions given above provide 9 equations for the 10 unknowns S_i, v_i, P_1, P_3 with $i = 1, 2, 3, 4$. *[511.2.2]* To close the system of equations the conditions $v_2 = 0$ or $v_4 = 0$ could be used. *[511.2.3]* These conditions apply when the nonpercolating phases are immobile as it is often observed in experiment. *[511.2.4]* It turns out, however, that there exists a less restrictive and, in our opinion, more natural selfconsistent closure.

[511.3.1] The selfconsistent closure condition used in this paper follows naturally from many limiting cases. *[511.3.2]* One such limit is the residual decoupling approximation close to hydrostatic equilibrium described in detail in [26, Section 5., p. 216ff]. *[511.3.3]* A second, more general limiting case is the limit of vanishing velocities, i.e. $v_i \to 0$ for

[a] Fig. 2 in [2] shows that the pressure measured by the pore pressure transducers PPT3 and PPT4 rebounds after the end of the infiltration, i.e. when the DNAPL has passed and the transducers measure the pressure of water and residual PCE

$i = 1, 2, 3, 4$. *[511.3.4]* Here we formulate the selfconsistent closure condition in its most general form as

$$\begin{aligned} 0 = \quad & \left(\frac{R_{13}}{\phi_1} + \frac{R_{14}}{\phi_1} + \frac{R_{15}}{\phi_1} + \frac{R_{31}}{\phi_3} - \frac{R_{41}}{\phi_4} + \frac{M_1}{\phi_1} \right) v_1 + \varrho_1 \frac{\mathrm{D}^1}{\mathrm{D}t} v_1 \\ & + \left(-\frac{R_{23}}{\phi_2} - \frac{R_{24}}{\phi_2} - \frac{R_{25}}{\phi_2} + \frac{R_{32}}{\phi_3} - \frac{R_{42}}{\phi_4} + \frac{M_1}{\phi_2} \right) v_2 - \varrho_2 \frac{\mathrm{D}^2}{\mathrm{D}t} v_2 \\ & + \left(-\frac{R_{13}}{\phi_1} + \frac{R_{23}}{\phi_2} - \frac{R_{31}}{\phi_3} - \frac{R_{32}}{\phi_3} - \frac{R_{35}}{\phi_3} - \frac{M_3}{\phi_3} \right) v_3 - \varrho_3 \frac{\mathrm{D}^3}{\mathrm{D}t} v_3 \\ & + \left(-\frac{R_{14}}{\phi_1} + \frac{R_{24}}{\phi_2} + \frac{R_{41}}{\phi_4} + \frac{R_{42}}{\phi_4} + \frac{R_{45}}{\phi_4} - \frac{M_3}{\phi_4} \right) v_4 + \varrho_4 \frac{\mathrm{D}^4}{\mathrm{D}t} v_4. \end{aligned} \tag{12}$$

[page 512, §1] *[512.2.1]* This condition follows selfconsistently from the constitutive theory. *[512.2.2]* It expresses the experimental observation that the pressure difference $P_3 - P_1$ depends more strongly on saturations than on velocities, and that it remains nonzero even for vanishing velocities. *[512.2.3]* Adding eqs. (3) for $i = 2$ and $i = 3$ and subtracting eqs. (3) with $i = 1$ and $i = 4$ from the result gives

$$\frac{\partial P_3}{\partial x} = \frac{\partial P_1}{\partial x} + \frac{\partial}{2\partial x} \left[\Pi_\mathrm{a} S_1^{-\alpha} - \Pi_\mathrm{b} S_3^{-\beta} + \gamma P_2^* S_2^{\gamma - 1} - \delta P_4^* S_4^{\delta - 1} \right]. \tag{13}$$

[512.2.4] In this form the selfconsistent closure has been used in the numerical calculation below.

[512.3.1] The mathematical model defined above was introduced and discussed in [24–26]. *[512.3.2]* It was recently extended to include surface tension [27]. *[512.3.3]* Notation and model formulation in this paper follow [26]. *[512.3.4]* Approximations and analytical solutions for some special cases were given in [24–26]. *[512.3.5]* Here the system of equations will be solved by numerical methods. *[512.3.6]* To this end initial and boundary conditions are needed and will be discussed next.

3. **Initial Conditions, Boundary Conditions and Model Parameters**

[512.4.1] Consider a cylindrical column containing a homogeneous, isotropic and incompressible porous medium. *[512.4.2]* The column is closed at both ends and filled with two immiscible fluids. *[512.4.3]* Assume that the surface and interfacial tensions are such that the capillary fringe is much thicker than the column diameter so that a onedimensional description is appropriate.

[512.5.1] The experimental situation considered here is that of raising a closed column as described in [26, p. 223]. *[512.5.2]* It is illustrated in Figure 1. *[512.5.3]* Initially, at instant $t = 0$, both fluids are at rest. *[512.5.4]* The column is oriented horizontally ($\vartheta = 0$), i.e., perpendicular to the direction of gravity. *[512.5.5]* The displacement processes are initiated by rotating the column into a vertical position. *[512.5.6]* The time protocol for rotating the column may generally be written as

$$\vartheta(t) = \arcsin\left\{\frac{1}{2}\left[\tanh\left(\frac{t - t_*}{t_{**}}\right) + 1\right]\right\} \tag{14}$$

where t_* is the instant of most rapid rotation and t_{**} is the inverse rate of the rotation.

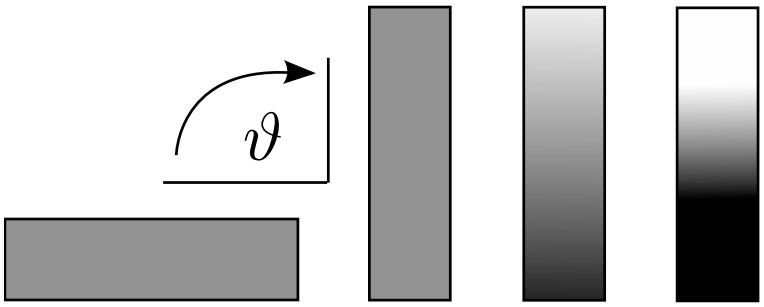

FIGURE 1. Raising a closed column according to the protocol of (14). Initially the column is oriented horizontally and the saturations are constant. Regions of high water saturation are indicated in darker shade, regions of high oil saturation are indicated in lighter shade. The last two columns illustrate the simultaneous imbibition (lower part of column) and drainage (upper part of column) processes that finally result in the formation of a capillary fringe.

[512.6.1] The constitutive equations yield the following system of 10 coupled nonlinear partial differential equations

$$\frac{\partial S_1}{\partial t} + \frac{\partial (S_1 v_1)}{\partial x} = \eta_2 \left(\frac{S_2 - {S_2}^*}{{S_{\mathbb{W}}}^* - S_{\mathbb{W}}} \right) \frac{\partial S_{\mathbb{W}}}{\partial t} \tag{15a}$$

$$\frac{\partial S_2}{\partial t} + \frac{\partial (S_2 v_2)}{\partial x} = -\eta_2 \left(\frac{S_2 - {S_2}^*}{{S_{\mathbb{W}}}^* - S_{\mathbb{W}}} \right) \frac{\partial S_{\mathbb{W}}}{\partial t} \tag{15b}$$

$$\frac{\partial S_3}{\partial t} + \frac{\partial (S_3 v_3)}{\partial x} = \eta_4 \left(\frac{S_4 - {S_4}^*}{{S_{\mathbb{O}}}^* - S_{\mathbb{O}}} \right) \frac{\partial S_{\mathbb{O}}}{\partial t} \tag{15c}$$

$$\frac{\partial S_4}{\partial t} + \frac{\partial (S_4 v_4)}{\partial x} = -\eta_4 \left(\frac{S_4 - {S_4}^*}{{S_{\mathbb{O}}}^* - S_{\mathbb{O}}} \right) \frac{\partial S_{\mathbb{O}}}{\partial t} \tag{15d}$$

$$\begin{aligned} &\varrho_{\mathbb{W}} \frac{\mathrm{D}^1}{\mathrm{D}t} v_1 + \frac{\partial P_1}{\partial x} - \varrho_{\mathbb{W}} g \sin\vartheta \\ &\qquad = \sum_{j=1}^{5} \frac{R_{1j}}{\phi S_1} (v_j - v_1) - \frac{\eta_2 v_1}{S_1} \left(\frac{S_2 - {S_2}^*}{{S_{\mathbb{W}}}^* - S_{\mathbb{W}}} \right) \frac{\partial S_{\mathbb{W}}}{\partial t} \end{aligned} \tag{15e}$$

$$\begin{aligned} &\varrho_{\mathbb{W}} \frac{\mathrm{D}^2}{\mathrm{D}t} v_2 + \frac{\partial}{\partial x} (P_3 - \gamma P_2^* S_2^{\gamma - 1} - \Pi_{\mathrm{a}} S_1^{-\alpha}) - \varrho_{\mathbb{W}} g \sin\vartheta \\ &\qquad = \sum_{j=1}^{5} \frac{R_{2j}}{\phi S_2} (v_j - v_2) + \frac{\eta_2 v_2}{S_2} \left(\frac{S_2 - {S_2}^*}{{S_{\mathbb{W}}}^* - S_{\mathbb{W}}} \right) \frac{\partial S_{\mathbb{W}}}{\partial t} \end{aligned} \tag{15f}$$

$$\begin{aligned} &\varrho_{\mathbb{O}} \frac{\mathrm{D}^3}{\mathrm{D}t} v_3 + \frac{\partial P_3}{\partial x} - \varrho_{\mathbb{O}} g \sin\vartheta \\ &\qquad = \sum_{j=1}^{5} \frac{R_{3j}}{\phi S_3} (v_j - v_3) - \frac{\eta_4 v_3}{S_3} \left(\frac{S_4 - {S_4}^*}{{S_{\mathbb{O}}}^* - S_{\mathbb{O}}} \right) \frac{\partial S_{\mathbb{O}}}{\partial t} \end{aligned} \tag{15g}$$

$$\begin{aligned} &\varrho_{\mathbb{O}} \frac{\mathrm{D}^4}{\mathrm{D}t} v_4 + \frac{\partial}{\partial x} (P_1 - \delta P_4^* S_4^{\delta - 1} - \Pi_{\mathrm{b}} S_3^{-\beta}) - \varrho_{\mathbb{O}} g \sin\vartheta \\ &\qquad = \sum_{j=1}^{5} \frac{R_{4j}}{\phi S_4} (v_j - v_4) + \frac{\eta_4 v_4}{S_4} \left(\frac{S_4 - {S_4}^*}{{S_{\mathbb{O}}}^* - S_{\mathbb{O}}} \right) \frac{\partial S_{\mathbb{O}}}{\partial t} \end{aligned} \tag{15h}$$

$$S_1 + S_2 + S_3 + S_4 = 1 \tag{15i}$$

$$\frac{\partial P_3}{\partial x} = \frac{\partial P_1}{\partial x} + \frac{\partial}{2\partial x} \left[\Pi_{\mathrm{a}} S_1^{-\alpha} - \Pi_{\mathrm{b}} S_3^{-\beta} + \gamma P_2^* S_2^{\gamma - 1} - \delta P_4^* S_4^{\delta - 1} \right] \tag{15j}$$

[page 513, §0] where $v_5 = 0, R_{12} = 0, R_{34} = 0$, and the quantities ${S_{\mathbb{W}}}^*, {S_{\mathbb{O}}}^*, {S_2}^*, {S_4}^*$ are defined in eq. (7). *[513.0.1]* This system of 10 equations is reduced to a system of only 9 equations by inserting eq. (15j) into eqs. (15f) and (15g) to eliminate $\partial P_3 / \partial x$. *[513.0.2]* The remaining 9 unknowns are $S_i, v_i, (i = 1, 2, 3, 4)$ and P_1.

[513.1.1] The system (15) has to be solved subject to initial and boundary data. *[513.1.2]* No flow boundary conditions at both ends require

$$v_i(0, t) = 0, \qquad i = 1, 2, 3, 4, \tag{16a}$$

$$v_i(L, t) = 0, \qquad i = 1, 2, 3, 4. \tag{16b}$$

[513.1.3] The fluids are incompressible. *[513.1.4]* Hence the reference pressure can be fixed to zero at the left boundary

$$P_1(0, t) = 0. \tag{17}$$

[513.1.5] The saturations remain free at the boundaries of the column.

[513.2.1] Initially the fluids are at rest and their velocities vanish. *[513.2.2]* The initial conditions are ($i = 1, 2, 3, 4$)

$$v_i(x, 0) = v_i^0(x) = 0 \tag{18a}$$

$$P_1 = P_1^0(x) = 0 \tag{18b}$$

$$S_i(x, 0) = S_i^0(x) = S_i^0. \tag{18c}$$

[513.2.3] In the present study the initial saturations will be taken as constants, i.e. independent of x.

[513.3.1] The model parameters are chosen largely identical to the parameters in [26]. *[513.3.2]* They describe experimental data obtained at the Versuchseinrichtung zur Grundwasser- und Altlastensanierung (VEGAS) at the Universität Stuttgart [40]. *[513.3.3]* The model parameters are $\varrho_{\mathbb{W}} = 1000\,\mathrm{kg\,m^{-3}}$, $\varrho_{\mathbb{O}} = 800\,\mathrm{kg\,m^{-3}}$, $\phi = 0.345$, $S_{\mathbb{W}\,\mathrm{i}} = 0.15$, $S_{\mathbb{O}\,\mathrm{r}} = 0.19$, $\eta_2 = 4$, $\eta_4 = 3$, $\alpha = 0.52$, $\beta = 0.90$, $\gamma = 1.5$, $\delta = 3.5$, $\Pi_{\mathrm{a}} = 1620\,\mathrm{Pa}$, $\Pi_{\mathrm{b}} = 25\,\mathrm{Pa}$, $P_2^* = 2500\,\mathrm{Pa}$ and $P_4^* = 400\,\mathrm{Pa}$. *[513.3.4]* In [26] only stationary and quasistationary solutions were considered, and the viscous resistance coefficients remained unspecified. *[513.3.5]* In order to *[page 514, §0]* find realistic values remember that $R_{31}+R_{41}+R_{15} = 2\mu_{\mathbb{W}}\phi^2/k$ [25,26]. *[514.0.1]* Realistic values for the viscosity and permeability are $\mu_{\mathbb{W}} = 0.0015\,\mathrm{kg\,m^{-1}\,s^{-1}}$ and $k = 10^{-12}\,\mathrm{m^{-2}}$. *[514.0.2]* Based on these orders of magnitude the viscous resistance coefficients are specified as $R_{13} = R_{31} = R_{14} = R_{41} = R_{23} = R_{32} = R_{24} = R_{42} = R_{15} = R_{35} = 1.7 \times 10^8\,\mathrm{kg\,m^{-3}\,s^{-1}}$, and $R_{25} = R_{45} = 1.7 \times 10^{10}\,\mathrm{kg\,m^{-3}\,s^{-1}}$.

[514.1.1] The column is filled with water having total saturation $S_{\mathbb{W}} = 0.45$ and oil with saturation $S_{\mathbb{O}} = 0.55$. *[514.1.2]* Two different initial conditions will be investigated that differ in relative abundance of the nonpercolating phase. *[514.1.3]* The saturations for initial condition A and B are in obvious notation given as

$$S_1^{0A} = 0.449, \qquad S_1^{0B} = 0.302 \tag{19a}$$

$$S_2^{0A} = 0.001, \qquad S_2^{0B} = 0.148 \tag{19b}$$

$$S_3^{0A} = 0.377, \qquad S_3^{0B} = 0.549 \tag{19c}$$

$$S_4^{0A} = 0.173, \qquad S_4^{0B} = 0.001. \tag{19d}$$

[514.2.1] These phase distributions can be prepared experimentally by an imbibition process for A or by a drainage process for inital condition B. *[514.2.2]* The values for the nonpercolating saturations were chosen from the nonpercolating saturations predicted within the residual decoupling approximation. *[514.2.3]* They can be read off from Figure 5 in [26]. *[514.2.4]* The values for the percolating phases follow from the requirement that the total water saturation is 0.45. *[514.2.5]* The time scales for raising the column are chosen as $t_* = 50\,000\,\mathrm{s}$ $t_{**} = 100\,000\,\mathrm{s}$ corresponding to roughly 3 hours.

4. **Numerical implemetation**

[514.3.1] The coupled system of nonlinear partial differential and algebraic equations is solved numerically using an adaptive moving grid solver [7,12,44]. *[514.3.2]* Its FORTRAN

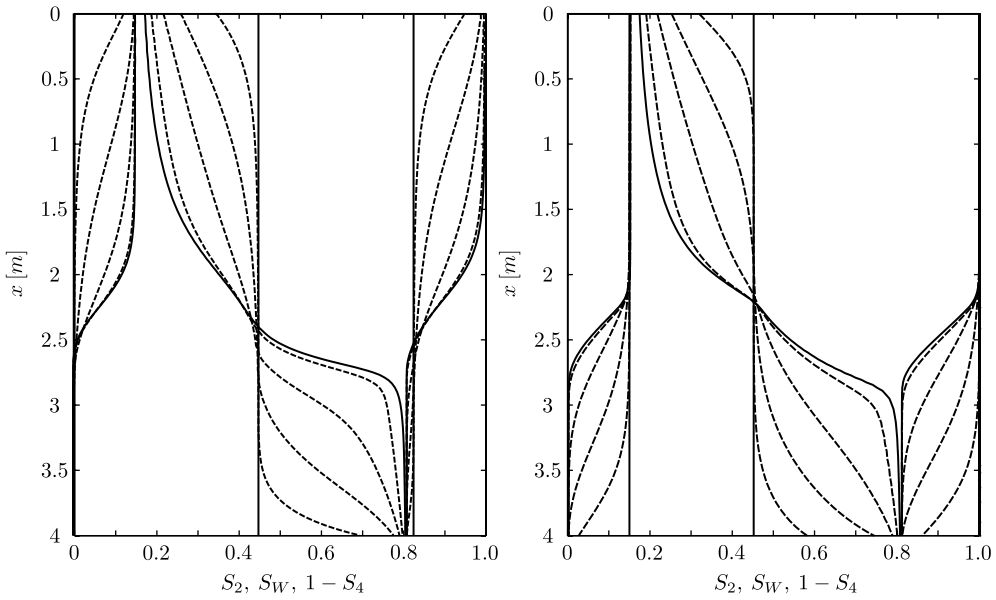

FIGURE 2. Approximate numerical solutions of eqs. (15) showing time evolution of saturation profiles $S_2(x,t)$, $S_{\mathbb{W}}(x,t)$, $1-S_4(x,t)$ at times $t=0\,\mathrm{s}$, $t=6\times10^6\,\mathrm{s}$ (solid lines) and $t=10^5, 2.5\times10^5, 5\times10^5, 7.5\times10^5\,\mathrm{s}$ (dashed lines) when raising a closed column of length $L=4\,\mathrm{m}$ from a horizontal to a vertical orientation. The left figure shows the time evolution starting from initial condition A in eq. (19), the right figure for initial condition B. Solid vertical lines correspond to $t=0$ when the column is horizontal. Dashed lines correspond to intermediate times. The first dashed line corresponding to instant $t=10^5\,\mathrm{s}$ is the time when the column has just reached a vertical orientation. Solid curves show the quasistationary solution for $t=6\times10^6\,\mathrm{s}$. While the upper part of the column is drained, imbibition takes place simultaneously in the lower part. Near $x=2.5\,\mathrm{m}$ drainage takes place initially but is later followed by imbibition.

implementation was described in [7]. *[514.3.3]* Space is discretized by finite differences. *[514.3.4]* The time integration within this algorithm is performed using the public domain differential algebraic solver DASSL, which is a higher order implicit backward Euler scheme.

[514.4.1] The mathematical model does not fit exactly the structure of the solver. *[514.4.2]* The following reformulations and adaptations had to be imposed: Elimination of time derivatives, regularizations of saturation, flux symmetrization, and pressure stabilization using the pressure projection method [10]. *[514.4.3]* In addition an adaptive algorithm contains parameters regulating the spatial smoothing or the adaptivity of the moving grid. *[514.4.4]* Details of the numerical implementation will be given elsewhere [15]. *[514.4.5]* Although a thorough sensitivity analysis with respect to all artifical parameters shows that the solutions are insensitive to the parameters over a wide range, it is clear that the numerical solutions presented below are approximate at best. *[514.4.6]* They are given mainly to illustrate qualitatively the differences between the present theory and the accepted traditional theory.

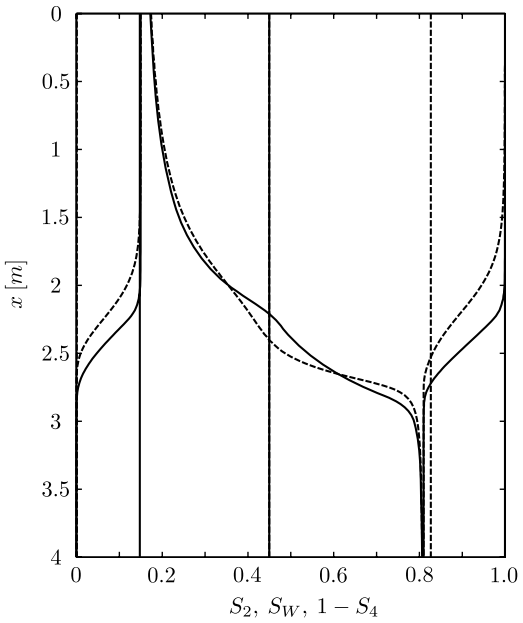

FIGURE 3. Initial ($t = 0$) and quasistationary ($t = 6 \times 10^6$ s) saturation profiles $S_i(x,t)$ as a function of height x after raising a closed column of length $L = 4$ m. Two triples of curves (solid and dashed) are shown. In each triple the leftmost curve shows $S_2(x)$, the center curve shows $S_{\mathbb{W}}(x)$ and the rightmost curve shows $1 - S_4(x)$. The triple of dashed vertical straight lines represents the saturation profile at $t = 0$ for initial condition A in eq. (19), while the triple of solid vertical lines represents initial condition B (the rightmost solid line and leftmost dashed line coincide almost with the bounding box). Note that the dashed and solid lines at $S = 0.45$ coincide. The triple of dashed curves represents the quasistationary saturation profile for $t \to \infty$ resulting from initial condition A, while the triple of solid curves represents the stationary saturation profile for $t \to \infty$ resulting from initial condition B. The figure illustrates that the quasistationary profiles depend strongly on the initial condition.

5. **Results**

[514.5.1] Figures 2 show the time evolution of the saturation profile starting from initial condition A (left figure) and initial condition B (right figure). *[514.5.2]* Time instants shown are $t = 0$s, $t = 6 \times 10^6$ s (solid lines) as well as $t = 10^5$ s, $t = 2.5 \times 10^5$ s, $t = 5 \times 10^5$ s and $t = 10^6$ s (dashed lines). *[514.5.3]* Gravity is oriented downward along the ordinate. *[514.5.4]* A complete saturation profile consists of three curves. *[514.5.5]* The leftmost curve of a triple is $S_2(x,t)$, the middle curve is $S_{\mathbb{W}}(x,t)$ and the rightmost curve is $1 - S_4(x,t)$. *[514.5.6]* From these curves the saturations are easily read off using eq. (1b). *[514.5.7]* Namely, at fixed height x the distance from the ordinate to the first curve of a triple represents $S_2(x)$, the distance between the first and the second curve represents $S_1(x)$, the distance between the second and the third represents $S_3(x)$ and the distance between the third curve and 1 represents $S_4(x)$. *[514.5.8]* The initial saturations at $t = 0$ correspond to vertical straight lines. *[514.5.9]* Subsequent profiles at $t = 10^5, 2.5 \times 10^5, 5 \times 10^5$ and 7.5×10^5 s are represented by four triples of dashed curves.

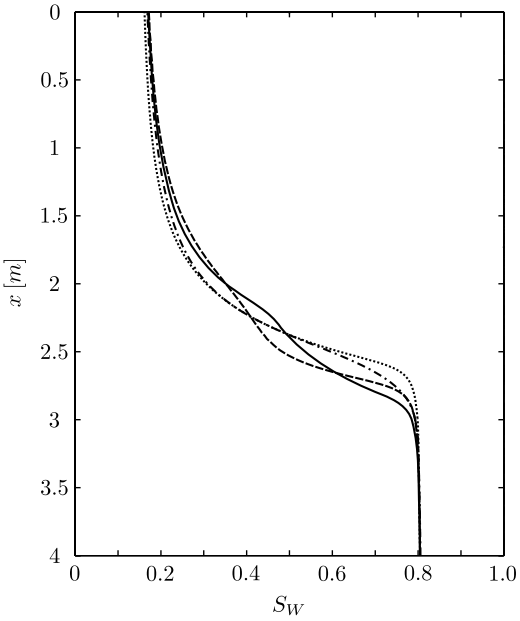

FIGURE 4. Comparison of the quasistationary water saturation curves shown in Figure 3 with the traditional theory for two phase flow. The dashed and solid curves are identical to the corresponding curves in Figure 3. The dashed-dotted curve shows the hydrostatic equilibrium calculated from eq. (20) using the appropriate secondary drainage capillary pressure function obtained in the residual decoupling approximation with the same parameters in [26]. The dotted curve shows the hydrostatic equilibrium water saturation profile calcluated from eq. (20) using the secondary imbibition capillary pressure function.

[514.5.10] The final quasistationary profile at $t = 6 \times 10^6$ s is represented by one triple of solid curves.

[514.6.1] At $t = 0$ the column is oriented horizontally, at $t = 10^5$ the column has just reached its vertical position. *[514.6.2]* As the water begins to imbibe the lower part of the column the upper part is simultaneously drained. *[514.6.3]* As the oil rises upward it merges with the residual oil and creates irreducible water (left figure). *[514.6.4]* Equivalently the process may be viewed as leaving behind residual oil (see the lower right corner of the right figure). *[514.6.5]* Similarly, the water falling to the bottom may be viewed as leaving behind irreducible water (see the upper left corner of the left figure), or as merging with the irreducible water thereby creating residual oil as seen in the right figure. *[514.6.6]* Note also that in the region around $x = 2.5$ m the process can change with time from drainage to imbibition. *[514.6.7]* Therefore, in the process of raising a closed column the nature of the displacement (imbibition vs. drainage) is not only position but also timedependent.

[page 515, §1] *[515.2.1]* Figure 3 compares the quasistationary ($t = 6 \times 10^6$ s) saturation profiles for different initial conditions. *[515.2.2]* Dashed lines and curves correspond to initial condition A in eq. (19), while solid lines and curves show results for initial condition B. *[515.2.3]* The straight vertical line at 0.45 is a double line. *[515.2.4]* It represents the initial water saturation of 0.45 for both initial conditions. *[515.2.5]* Figure 3 shows a strong dependence on the initial distribution of nonpercolating fluids. *[515.2.6]* In particular the nonpercolating nonwetting fluid depends strongly on the initial condition. *[515.2.7]* Initial condition A represents a fluid distribution that could ensue after an imbibition, while initial condition B could be realistic after a drainage.

[515.3.1] Figure 4 illustrates the differences between the present theory and the traditional theory. *[515.3.2]* It shows the two quasistationary profiles (solid and dashed middle curves) as in Figure 3 calculated dynamically from the present theory and compares them to

stationary solutions of the traditional theory based on the capillary pressure concept. *[515.3.3]* In the traditional theory the water saturation in hydrostatic equilibrium in a vertical column is given as [5]

$$S_{\mathbb{W}}(x) = P_{\mathrm{c}}^{-1}(C + (\varrho_{\mathbb{O}} - \varrho_{\mathbb{W}})gx) \tag{20}$$

where P_{c} is the capillary pressure and C an integration constant. *[515.3.4]* In view of the boundary conditions (closed column) the integration constant is fixed such that

$$\int_0^L S_{\mathbb{W}}(x)\mathrm{d}x = 0.45L \tag{21}$$

[page 516, §0] is the total water volume. *[516.0.1]* The dash-dotted curve in Figure 4 is obtained in this way by specifying for P_{c} the appropriate secondary drainage curve for the porous medium. *[516.0.2]* This secondary drainage curve was obtained in [26] and can be seen in Figure 1 of [26]. *[516.0.3]* The dotted curve in Figure 4 is obtained by specifying for P_{c} the secondary imbibition curve for the medium. *[516.0.4]* This imbibition curve can be seen also in Figure 1 of [26]. *[516.0.5]* The comparison shows that the quasistationary solutions obtained from eqs. (15) differ significantly in the region of the capillary fringe from the equilibrium profiles predicted by the traditional theory.

6. Conclusion

[516.1.1] Numerical solutions were calculated for the coupled system (15) of nonlinear partial differential equations obtained by macroscopic constitutive modeling of two phase flow. *[516.1.2]* The equations are based on the concept of hydraulic percolation of fluid phases. *[516.1.3]* The results illustrate the ability of the new theory to describe drainage and imbibition occurring simultaneously within the same sample, or sequentially at the same position inside a porous medium. *[516.1.4]* Stationary solutions are compared to predictions from the traditional theory and significant differences are found. *[516.1.5]* We emphasize that the numerical solutions are approximate. *[516.1.6]* We encourage experimental groups to measure residual fluid distributions during or after immiscible displacement. *[516.1.7]* Such measurements would allow us to test our theoretical predictions against experiment.

Acknowledgement

The authors thank P. Zegeling for many fruitful discussions. They are grateful to the Deutsche Forschungsgemeinschaft and the International Research and Training Group on Nonlinearities and Upscaling (IRTG NUPUS) for financial support.

References

[1] Abrams, A.: The influence of fluid viscosity, interfacial tension, and flow velocity on residual oil left by waterflood. Soc. Petr. Eng. Journal **15**, 437 (1975)

[2] Ataie-Ashtiani, B., Hassanizadeh, S., Oung, O., Westrate, F., Bezuijen, A.: Numerical modelling of two-phase flow in a geocentrifuge. Environmental Modeling and Software **18**, 231 (2003)

[3] Avraam, D.G., Payatakes, A.C.: Generalized relative permeability coefficients during steady-state two-phase flow in porous media, and correlation with the flow mechanisms. Transport in Porous Media **20**, 135 – 168 (1995)

[4] Avraam, D.G., Payatakes, A.C.: Flow mechanisms, relative permeabilities and coupling effects in steady-state two-phase flow through porous media. the case of strong wettability. Industrial Engineering Chemistry Research **38**, 778 – 786 (1999)

[5] Bear, J.: Dynamics of Fluids in Porous Media. Elsevier Publ. Co., New York (1972)

[6] Bear, J., Braester, C., Menier, P.: Effective and relative permeabilities of anisotropic porous media. Transport in Porous Media **2**, 301 (1987)

[7] Blom, J., Zegeling, P.: Algorithm 731: A moving-grid interface for systems of one-dimensional time-dependent partial differential equations. ACM Transactions in Mathematical Software **20**, 194 (1994)

[8] Blunt, M., King, M., Scher, H.: Simulation and theory of two-phase flow in porous media. Phys. Rev. A **46**, 7680 (1992)

[9] Bryant, S., Mellor, D., Cade, C.: Physically representative network models of transport in porous media. AIChE Journal **39**, 387 (1993)

[10] Chorin, A.: A numerical method for solving incompressible viscous flow problems. J.Comp.Phys. **2**, 12 (1967)

[11] Collins, R.: Flow of Fluids through Porous Materials. Reinhold Publishing Co., New York (1961)

[12] Dam, A., Zegeling, P.: A robust moving mesh finite volume method applied to 1d hyperbolic conservation laws from magnetohydrodynamics. Journal of Computational Physics **216**, 526 (2006)

[13] Dias, M., Payatakes, A.: Network models for two-phase flow in porous media I: Immiscible microdisplacement of non-wetting fluids. J. Fluid Mech. **164**, 305 (1986)

[14] van Dijke, M., Sorbie, K.: Pore-scale network model for three-phase flow in mixed-wet porous media. Phys.Rev.E **66**, 046,301 (2002)

[15] Doster, F., Zegeling, P., Hilfer, R.: Numerical solutions of a generalized theory for macroscopic capillarity (2008)

[16] Dullien, F.: Porous Media - Fluid Transport and Pore Structure. Academic Press, San Diego (1992)

[17] Fatt, I.: The network model of porous media I. capillary pressure characteristics. AIME Petroleum Transactions **207**, 144 (1956)

[18] Ferer, M., Bromhal, G., Smith, D.: Pore-level modeling of drainage: Crossover from invasion percolation fingering to compact flow. Phys.Rev.E **67**, 051,601 (2003)

[19] Gardescu, I.: Behavior of gas bubbles in capillary spaces. Trans. AIME **136**, 351 (1930)

[20] Helmig, R.: Multiphase Flow and Transport Processes in the Subsurface. Springer, Berlin (1997)

[21] Hidajat, I., Rastogi, A., Singh, M., Mohanty, K.: Transport properties of porous media from thin-sections (2001). Paper SPE69623 presented 2001 at the SPE Latin American and Carribean Petroleum Engineering Conference, Buenos Aires, Argentina

[22] Hilfer, R.: Transport and relaxation phenomena in porous media. Advances in Chemical Physics **XCII**, 299 (1996)

[23] Hilfer, R.: Macroscopic equations of motion for two phase flow in porous media. Physical Review E **58**, 2090 (1998)

[24] Hilfer, R.: Capillary pressure, hysteresis and residual saturation in porous media. Physica A **359**, 119 (2006)

[25] Hilfer, R.: Macroscopic capillarity and hysteresis for flow in porous media. Phys.Rev.E **73**, 016,307 (2006)

[26] Hilfer, R.: Macroscopic capillarity without a constitutive capillary pressure function. Physica A **371**, 209 (2006)

[27] Hilfer, R.: Modeling and simulation of macrocapillarity. In: Garrido, P., Hurtado, P., Marro, J. (eds.) CP1091, Modeling and Simulation of Materials, p. 141. American Institute of Physics, New York (2009)

[28] Hilfer, R., Besserer, H.: Macroscopic two phase flow in porous media. Physica B **279**, 125 (2000)

[29] Hilfer, R., Besserer, H.: Old problems and new solutions for multiphase flow in porous media. In: Dmitrievsky, A., Panfilov, M. (eds.) Porous Media: Physics, Models, Simulation, p. 133. World Scientific Publ. Co., Singapore (2000)

[30] Jamin, J.: Memoire sur l'equilibre et le mouvement des liquides dans les corps poreux. Comptes Rendus Academie de Sciences de France **50**, 172 (1860)
[31] Jerauld, G., Salter, S.: The effect of pore structure on hysteresis in relative permeability and capillary pressure: Pore level modeling. Transport in Porous Media **5**, 103 (1990)
[32] Marsily, G.: Quantitative Hydrogeology – Groundwater Hydrology for Engineers. Academic Press, San Diego (1986)
[33] McKellar, M., Wardlaw, N.: A method of making two dimensional glass micromodels of pore sytems. J. Cdn. Pet. Tech. **21**, 39 (1982)
[34] Øren, P., Billiotte, J., Pinczewski, W.: Mobilization of waterflood residual oil by gas injection for water wet conditions. SPE Formation and Evaluation **March 1992**, 70 (1992)
[35] Oxaal, U.: Fractal viscous fingering in inhomogeneous porous models. Phys. Rev. A **44**, 5038 (1991)
[36] Oxaal, U., Boger, F., Feder, J., Jøssang, T., Meakin, P., Aharony, A.: Viscous fingering in square lattice models with two types of bonds. Phys. Rev. A **44**, 6564 (1991)
[37] Payatakes, A.: Dynamics of oil ganglia during immiscible displacement in water-wet porous media. Ann.Rev.Fluid Mech. **14**, 365 (1982)
[38] Payatakes, A., Neira, M.: Model of the constricted unit cell type for isotropic granular porous media. AIChE Journal **23**, 922 (1977)
[39] Scheidegger, A.: The Physics of Flow Through Porous Media. University of Toronto Press, Canada (1957)
[40] Sheta, H.: Simulation von Mehrphasenvorgängen in porösen Medien unter Einbeziehung von Hysterese-Effekten. Ph.D. thesis, Institut für Wasserbau, Universität Stuttgart (1999)
[41] Taber, J.: Dynamic and static forces required to remove a discontinuous oil phase from porous media containing both oil and water. Soc.Petr.Eng. Journal **9**, 3 (1969)
[42] de Wiest, R.: Flow Through Porous Media. Academic Press, New York (1969)
[43] Wyckoff, R., Botset, H.: Flow of gas-liquid mixtures through unconsolidated sands. Physics **7**, 325 (1936)
[44] Zegeling, P., Blom, J.: An evaluation of the gradient weighted moving finite element method in one space dimension. Journal of Computational Physics **103**, 422 (1992)